Spin-density wave in Cr: Nesting versus low-lying thermal excitations

Veerle Vanhoof,[1] Michel Rots,[1] and Stefaan Cottenier[1,2,*]
[1]*Instituut voor Kern- en Stralingsfysica and INPAC, K.U. Leuven, Celestijnenlaan 200 D, BE-3001 Leuven, Belgium*
[2]*Center for Molecular Modeling, Ghent University, Technologiepark 903, BE-9052 Zwijnaarde, Belgium*
(Received 20 August 2009; revised manuscript received 18 October 2009; published 19 November 2009)

It is well known that present versions of density functional theory do not predict the experimentally observed spin-density wave state to be the ground state of Cr. Recently, a so-called "nodon model" has been proposed as an alternative way to reconcile theory and experiment: the ground state of Cr is truly antiferromagnetic, and the spin-density wave appears due to low-lying thermal excitations ("nodons"). We examine in this paper whether the postulated properties of these nodons are reproduced by *ab initio* calculations.

DOI: 10.1103/PhysRevB.80.184420 PACS number(s): 75.50.Ee, 75.30.Fv, 71.20.Be

I. INTRODUCTION

Among all elemental solids, bcc Cr takes a peculiar position. It is the only light to medium-heavy element for which density functional theory (DFT) at the local-density approximation (LDA) or generalized gradient approximation (GGA) level predicts the wrong ground state for the elemental solid: antiferromagnetic (AF) bcc instead of the experimentally found bcc crystal with an antiferromagnetic spin-density wave (SDW) type of magnetic order. This SDW state is experimentally characterized as a wave modulation of the antiparallel Cr moments, with amplitude of 0.62 μ_B and wavelength $\lambda=61.3$ Å near 0 K (42.6 monolayers, incommensurate with the lattice) and the wave vector parallel to the [001] direction.[1,2] Neighboring Cr atoms have opposite spin moments. Below 123 K, the moments are parallel to the wave vector (longitudinal SDW); above that temperature they are perpendicular to it (transverse SDW). Above 311 K, the antiferromagnetic order is lost. The occurrence of this SDW state is a text book example[3,4] of the nesting mechanism, originally proposed by Overhauser[5] and Lomer:[6] if the product between the static susceptibility $\chi(\vec{q})$ of the paramagnetic state and a suitably defined intra-atomic exchange integral I (Stoner integral) exceeds unity, then the paramagnetic state is instable against the formation of a wave-modulated magnetic state with $\vec{q}$ as wave vector. This condition will be fulfilled if there are sufficiently large parts of the Fermi surface that can be translated into one another by the vector $\vec{q}$, which is in this context called a nesting vector. The nesting criterium is a generalization of the well-known Stoner criterium for the occurrence of ferromagnetism: if the product between the static uniform susceptibility $\chi(\vec{0})$ of the paramagnetic state and the Stoner integral I exceeds unity, then the paramagnetic state is instable against the formation of a ferromagnetic state. The uniform static susceptibility is related to the density of states at the Fermi energy, which leads to the usual formulation of the Stoner criterium: if the density of states at the Fermi energy in the paramagnetic state is sufficiently large, then the ferromagnetic state will have a lower total energy. Note that the nesting and Stoner criteria do not give a *sufficient* condition for the modulated or ferromagnetic state to appear: although the latter must have an energy lower than the paramagnetic state if the criterium is satisfied, it is not excluded that yet another type of state has an even lower energy. These criteria are neither a *necessary* condition for the appearance of the modulated or ferromagnetic state: if a potential barrier separates the nonmagnetic state and a modulated or ferromagnetic ground state, then the criteria are not fulfilled while nevertheless the modulated or ferromagnetic state can have a lower energy.

In the case of Cr, inspection of the Fermi surface[6–10] led to the conclusion that the nesting condition is fulfilled and that consequently the wave-modulated antiferromagnetic state should have a lower energy than the paramagnetic state. This is consistent with the experimental observation of the SDW. However, density functional theory at the LDA and GGA levels consistently predicts the unmodulated antiferromagnetic state to have an even lower energy.[11–13] This was interpreted as a problematic failure of LDA or GGA. It prompted several *ab initio* investigations of SDW Cr and attempts to reconcile theory and experiment.[7–10,14–21] Some time ago, a remarkable solution to the conflict was put forward by Uzdin and Demangeat[22] based on a model Hamiltonian study [periodic Anderson model (PAM)]. It builds further upon ideas that were in an embryonic form formulated in the work of Hafner *et al.*[8,9] Their argument goes as follows. Observing the three facts that (1) the nesting mechanism lowers the energy of the SDW state with respect to the nonmagnetic state,[5,6] (2) all DFT calculations yield a Fermi surface with the correct nesting properties,[9–11] and (3) the DFT-calculated energy of the SDW state is nevertheless higher than the AF energy, they do *not* conclude that the DFT energies are wrong (as was the common interpretation so far) but rather that nesting cannot be the ultimate driving mechanism for the occurrence of the SDW in Cr. By their PAM analysis, Uzdin and Demangeat proposed an alternative model based on low-lying quasiparticle excitations—the nodon model—that is in agreement both with experimental observations and with the *ab initio* total energies.

The goals of the present paper are to make the key ideas that are present in the work of Uzdin and Demangeat[22] more explicit and to give careful arguments for these ideas based on experiment, existing and new interpretations of their model Hamiltonian results, and new *ab initio* calculations. We will demonstrate that several but not all features of the nodon model are consistent with *ab initio* results. It is too early for a final judgment on the value of the nodon model for describing the magnetism of Cr, but the present analysis will hopefully stir the discussion.

II. COMPUTATIONAL DETAILS

We applied the full-potential augmented plane wave +local orbital (APW+lo) method[23–25] within the density functional theory,[25–27] as implemented in the WIEN2K package.[28] The LDA,[26,27,29–31] Perdew-Burke-Ernzerhof,[32] and LDA+U exchange-correlation (XC) functionals were used, the latter in the "around the mean-field" formulation by Czyżyk and Sawatzky.[33]

The wave functions in the APW+lo method are expanded in spherical harmonics within nonoverlapping muffin tin spheres of radius R_{MT} and in plane waves in the interstitial region. We took $R_{MT}(\mathrm{Cr})=2.1$ bohr radii (a_0). The spherical harmonics expansion in the spheres was truncated at $\ell_{max}=10$. For the plane wave expansion in the interstitial region, a truncation at $K_{max}=9.0/R_{MT}^{min}$ is needed for complete convergence of the magnetic moment. An acceptable accuracy (deviation of 0.03 μ_B) was reached with $K_{max}=6.5/R_{MT}^{min}$ for the computationally more demanding calculations of the spin-density wave. All reported data have been obtained from calculations with $K_{max}=7.0/R_{MT}^{min}$ (small bcc-unit cell, $1\times1\times20$ supercell, and intermediate supercells) or $K_{max}=6.5/R_{MT}^{min}$ ($2\times2\times20$ supercell). Energy differences are accurate and an error of 0.03 μ_B has to be taken into account for magnetic moments. The charge density in the interstitial region was expanded up to $G_{max}=16\sqrt{\mathrm{Ry}}$. The meshes of special k points in the irreducible Brillouin zone were set to $21\times21\times21$ for the small bcc-unit cell and to $21\times21\times1$ for the $1\times1\times20$ SDW supercell. For all intermediate supercell sizes equivalent k meshes were used. Following a suggestion in Ref. 10, it was verified that spin-orbit coupling does not significantly influences the energy differences between nonmagnetic, antiferromagnetic, and SDW Cr. Also the effect of spin-orbit coupling on the magnetic moment was tested to be negligibly small (0.005 μ_B). All calculations were therefore performed without spin-orbit coupling. As a consequence, the calculations are not sensitive to the polarization of the SDW.

III. CHOOSING AN XC FUNCTIONAL

Earlier work has made it clear that both LDA and GGA have their shortcomings for describing SDW Cr.[8,9,21] We will summarize these deficiencies in the present section and use this as a basis to propose LDA+U as a useful pragmatic alternative. In this part, we limit ourselves to the nonmagnetic and simple antiferromagnetic states, which are computationally much easier to treat and are sufficient to highlight the main features of the various functionals.

For LDA as well as GGA the nonmagnetic and the antiferromagnetic energy-versus-volume curves[8,9,18,21] behave qualitatively identical (Fig. 1), with a magnetic moment that goes asymptotically to zero for low volumes and a splitting of the two curves at higher volumes, with the antiferromagnetic curve lowest in energy. However, the lowest-energy equilibrium lattice constant (indicated by the arrows in Figs. 1 and 2) and magnetic moment (shown as a function of lattice constant in Fig. 2) are different for the two methods. In the case of LDA only the nonmagnetic state is present at the equilibrium lattice constant of 2.79 Å, while at the experimental lattice constant (2.88 Å) the antiferromagnetic state is present with a magnetic moment of 0.45 μ_B. The experimental magnetic moment of 0.62 μ_B is reached at 2.89 Å.

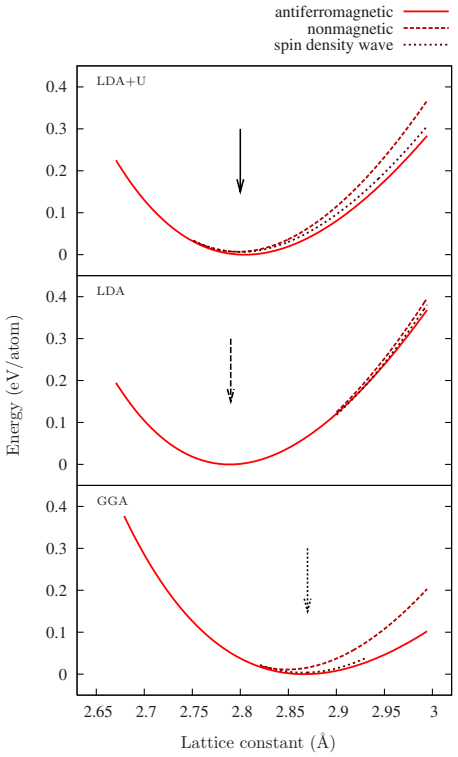

FIG. 1. (Color online) Murnaghan fits of the total energy as a function of lattice constant for nonmagnetic and simple antiferromagnetic Cr and for the SDW, calculated with GGA, LDA, and LDA+U. The full, dashed, and dotted arrows point at the equilibrium lattice constant for the LDA+U, LDA, and GGA methods, respectively. For each method, the energy at the equilibrium volume is taken to be zero and seven calculated points were used for each fit.

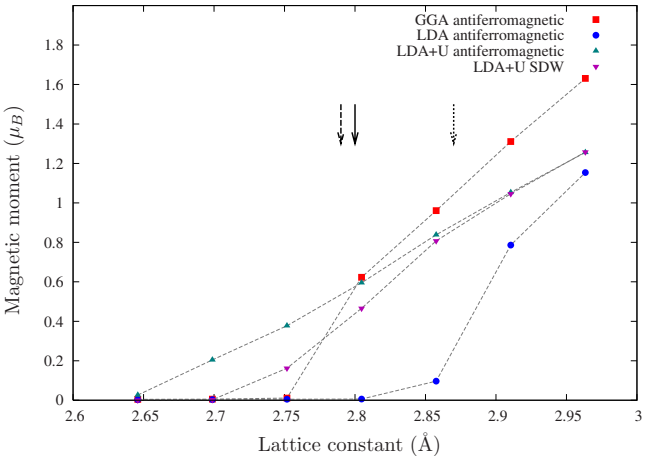

FIG. 2. (Color online) Magnetic moment as a function of lattice constant for the simple antiferromagnetic Cr and the SDW, calculated with GGA, LDA, and LDA+U. The full, dashed, and dotted arrows point at the equilibrium lattice constant for the LDA+U, LDA, and GGA method, respectively.

For GGA the antiferromagnetic state exists at an equilibrium lattice constant of 2.87 Å, which is rather close to the experimental value, but the corresponding magnetic moment of 1.02 μ_B is almost twice as large as the experimental one. In principle these lattice constants and magnetic moments should not be comparable to the experimental values since the SDW is known to be the experimental ground state, but previous calculations[21] have shown that the values for simple antiferromagnetic and SDW calculations do not differ too much, justifying the comparison. We can summarize by saying that LDA finds the experimental magnetic moment in the neighborhood of the experimental lattice constant but not at its own equilibrium, while GGA gives a lattice constant comparable with the experimental value but with a magnetic moment that is twice too large: none of both therefore gives a satisfactory description of Cr. The behavior of these two functionals is very similar to what is found in other 3*d* transition metal compounds as, e.g., Fe_4N.[34]

The LDA+U functional provides an alternative. LDA+U is a semi–*ab initio* method built on LDA but containing two additional free parameters: U (related to on-site Coulomb repulsion or electron correlation) and J (related to intra-atomic exchange). The idea is that LDA can be "upgraded" to describe the atomiclike correlation and exchange in strongly correlated systems by adding terms to the Hamiltonian that are known to describe this correlation and exchange well in the limit of free atoms. The (unknown) portion of correlation and exchange that is already present in LDA is counted twice and has to be subtracted. Various flavors of LDA+U exist, depending on how the parametrization and the double counting correction are chosen. We do not pretend bcc Cr to be a strongly correlated system, and strictly spoken the use of LDA+U is "illegal" here. But the possibility to vary the parameters U and J offers the freedom to make small modifications to the functional. This freedom is perhaps sufficient to remediate those features of LDA that lead to its incorrect predictions. As is suggested[28] for LDA+U, we take $J=0$ (acknowledging that LDA describes exchange sufficiently well). By tuning the value of U, we "fit" the magnetic moment of Cr to the experimental value. The spirit of this approach is comparable to another remedy to the shortcomings of LDA or GGA for Cr that was proposed before,[21,35] namely, tuning the lattice constant until the experimental magnetic moment is obtained.

For a value of $U=0.30$ Ry (4.1 eV) we obtain a magnetic moment of 0.59 μ_B at the equilibrium lattice constant of 2.81 Å, as can be seen in the energy and magnetic moment versus lattice constant curves presented in Figs. 1 and 2. This value is within its error range of 0.03 μ_B (see Sec. II) consistent with the experimental value of 0.62 μ_B. Although such a value for U is not really small for a 3*d* metal,[36] none of the properties of Cr we have inspected appears to be alarmingly wrong. This justifies the hope that the band structure obtained in this way is not unphysical. LDA+U succeeds in manipulating the magnetic moments by shifting the sublevels of a specified band, in this case the *d* band, over an energy range determined by their population. The effect is visible in the density of states plotted in Fig. 3. With respect to the LDA and GGA densities of states, which have a similar shape, the density of states for LDA+U shows a pronounced rearrangement of several peaks resulting in a narrowed band with altered shape. As a consequence of this rearrangement, the number of up and down electrons can change, thus resulting in a different magnetic moment. Different U parameters correspond to different shifts and will therefore yield different magnetic moments. Additionally, Fig. 1 reveals that applying LDA+U induces a small shift (0.02 Å) on the equilibrium lattice constant of LDA.

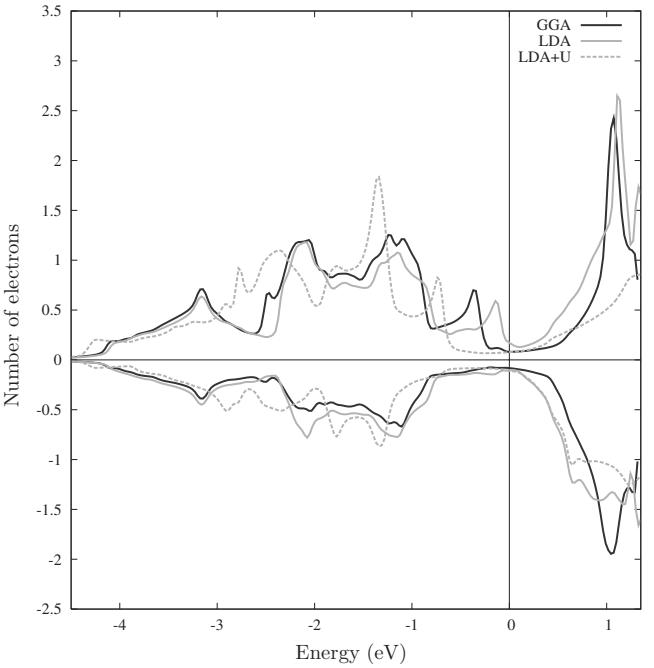

FIG. 3. The densities of states for the up and down electrons of the *d* band are shown for LDA, GGA, and LDA+U. On the y axis the number of up electrons is represented with a positive number of electrons, the number of down electrons with a negative number.

In conclusion, by using a moderate value of $U=0.30$ Ry, we have now a method that yields at its equilibrium volume a magnetic moment that is comparable to experiment. Moreover, this equilibrium volume is sufficiently close to the experimental volume. Although constructed on pragmatic grounds, this functional can therefore be expected to be more physically correct for Cr than LDA or GGA.

IV. SPIN-DENSITY WAVE AND NODON MODEL

Now we turn to the spin-density wave. In principle, if we want to obtain the SDW state of Cr with LDA+U, we should repeat the tuning of U: the magnetic moment known from experiment is the amplitude of the spin-density wave and not the simple antiferromagnetic moment. This is for practical reasons not feasible (many expensive LDA+U calculations for the SDW state would be needed). Consequently, the previous value for U was used. This leads, in the case of Cr, to a magnetic moment amplitude of 0.47 μ_B (Fig. 2) which is about 0.15 μ_B smaller than the experimental moment, indicating that a somewhat higher U is required to reach the experimental SDW amplitude at the equilibrium lattice constant. However, the interpretation of our results will not be affected by small deviations of U.

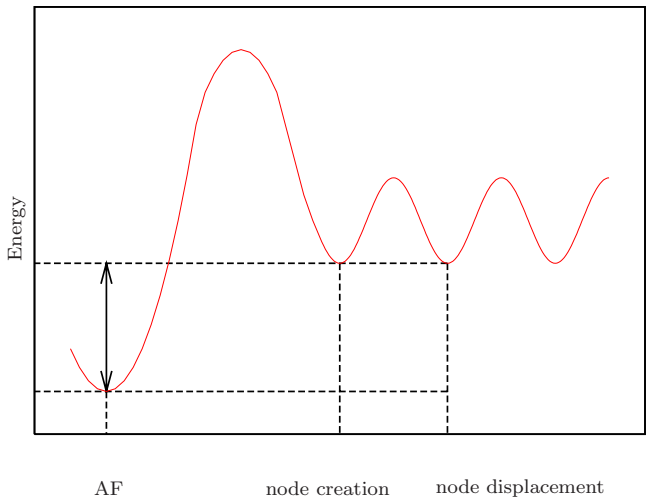

FIG. 4. (Color online) Qualitative sketch of the potential barriers for the formation and displacement of a nodon: once a nodon has been created, it takes less energy to displace it rather than to destroy it. The double-sided arrow indicates the *lower bound* for the energy needed to create an individual node [50–150 meV/nodon or 20–80 K (Sec. IV B)].

LDA and GGA obtain the simple antiferromagnetic configuration as ground state instead of the experimental spin-density wave ground state.[7–9,11–16,19–21] Figure 1 shows that also for LDA+U the simple antiferromagnetic configuration has the lowest energy, with an equilibrium lattice constant of 2.80 Å (Fig. 1) and a magnetic moment of 0.47 μ_B (Fig. 2). In this respect, LDA+U has the same "defect" as all other functionals. In their new interpretation Uzdin and Demangeat[22] suggested, however, that this is not a defect at all. Before we examine their idea in more detail, we note that the lower energy of the AF state is not forbidden by the nesting mechanism described in Sec. I of this paper. Indeed, as can be seen in the energy versus lattice constant curve in Fig. 1, the modulated state has a lower energy than the nonmagnetic state, which is exactly what the nesting mechanism prescribes. This does not exclude the possibility that another state—in this case simple AF—has an even lower energy.

We will now describe the hypothesis of Uzdin and Demangeat,[22] and in the remainder of this paper confront it with, among others, our LDA+U calculations. They claim that *the ground state of Cr is really antiferromagnetic* and is correctly predicted by DFT. However, this ground state is not experimentally observed. They explain this inconsistency by assuming the existence of quasiparticle excitations (one could call them "nodons") that can be populated already at very low temperatures. Each nodon corresponds to the introduction of one node (a lattice site with zero moment) in the antiferromagnetic Cr lattice. Such a node does not need to be localized but can travel through the Cr lattice. These nodons are claimed to have the following properties. (1) They can easily be created, but it is difficult to destroy them—this asymmetry can be understood by assuming potential barriers for the formation and displacement of a nodon as sketched qualitatively in Fig. 4: once a nodon is created, it is much easier to displace it than to destroy it (Uzdin and Demangeat[22] used the analogy of the rumpled surface for this). (2) The nodon-nodon interaction is highly anisotropic. In all directions perpendicular to [001] the interaction is strongly repulsive for distances smaller than the nearest-neighbor Cr-Cr distance and attractive for all other distances. Along the [001] direction, the interaction is weakly repulsive as soon as the distance between the nodes is larger than about 15 monolayers. (3) When two nodons approach each other along the [001] direction, they completely annihilate each other and locally the AF state is restored.

With these three features, Uzdin and Demangeat explained the existence of the SDW in Cr as follows. Cr really has the simple antiferromagnetic structure at 0 K. As soon as the temperature rises above an unknown but very small threshold, there is a chance that thermal fluctuations excite a nodon. Once it is there, it is unlikely to be destroyed, and it starts traveling through the lattice. The number of nodons continuously increases, and they start to interact with each other. The attractive interaction in the (001) plane will lead to the building of (001) planes of nodes. Once these planes are formed, one can resort to a one-dimensional picture of node planes that travel along the [001] direction. In such a one-dimensional description, the word nodon refers to an entire node plane rather than to an individual site with zero moment. The node planes repel each other along the [001] direction and therefore try to maximize their mutual distance along this direction. As meanwhile the creation of nodes continues, ever more planes will be formed and the [001] distance between planes decreases, leading to occasional annihilations when planes come too closely together. This evolution will come to an end when the formation and the annihilation of planes are in equilibrium. Due to the repulsive interaction, we end up with a collection of (001) node planes at regular distances from each other, which is nothing more than the SDW. If temperature rises, the creation of nodes becomes more likely again and extra node planes will be formed. These are now so densely packed that more annihilations take place, and the net result is *less* node planes, at larger distances from each other, in dynamic equilibrium with the formation of new nodes. This agrees with the experimental observation that the SDW wavelength increases with temperature.

Although this point of view used to understand the formation of the SDW has some attractive features, its validity depends entirely on the validity of the three claimed properties of the nodons. In the next sections we will confront these three properties with *ab initio* calculations and examine whether they are compatible with the latter or not.

A. Nature and range of the node-node interaction

1. Results by Uzdin and Demangeat

In this section we will reconstruct and/or make more explicit the argumentation by Uzdin and Demangeat[22] that leads to the conclusions that a node layer perturbs the Cr moments over a distance of 18 monolayers (c), that two node layers do not interact when they are separated by more than 24 monolayers (d), that there must be a separation distance smaller than this at which two node layers repel each other

(a), and finally that even smaller distances between two node layers lead to mutual annihilation (b).

(a) *A distance exists at which two node layers repel each other.* Indeed, if node planes would attract each other at all distances, then they would readily annihilate each other and a stable SDW would never exist. This does not mean, however, that repulsion occurs at *all* distances [see also (b)].

(b) *At sufficiently small distances, two node layers annihilate each other.* Within their PAM model, Uzdin and Demangeat can stabilize waves with a wavelength smaller than about 40 monolayers only if a modulated external field is present. When that field is switched off, the wave disappears again, indicating that the system can lower its energy by getting rid of the closely spaced node planes and restoring the antiferromagnetic configuration (=annihilation). For larger wavelengths, the wave solution survives without external field. This critical wavelength of 40 monolayers (20 monolayers between two node planes) is almost identical to the experimental wavelength of the SDW.

(c) *A node layer perturbs the Cr moments over a distance of 18 monolayers.* Uzdin and Demangeat showed in their paper pictures of spin-density waves for three different wavelengths λ (40, 80, and 120 monolayers). Since all waves are constructed from the same initial antiferromagnetic configuration with a magnetic moment of about 0.6 μ_B, one expects that the influence of a node plane on the surrounding magnetic moments will be the same in all cases. Visual inspection shows, for the two longest wavelengths, that the neighboring Cr moments are perturbed up to 18 monolayers away from each node. A similar analysis is not possible for the shortest wavelength because the nodes are only 20 monolayers apart and the perturbation ranges of two neighboring nodes overlap.

Although one could expect that two node planes start to interact with each other as soon as their perturbation ranges start to overlap [i.e., a node separation of $2\times18=36$ monolayers (wavelength $\lambda=72$ monolayers, $q/a^*=0.986$)], it turns out they can come much closer to each other before the interaction starts [see (d)].

(d) *Two node layers start to interact when they are separated by 24 monolayers or less.* In the inset of Fig. 5, we plot the (modified[37]) data of Uzdin and Demangeat for $E_{\mathrm{SDW}}-E_{\mathrm{AF}}$ (in meV/atom) as a function of q/a^*. Straightforward algebra shows that in such a plot this energy difference should depend linearly on q/a^* as long as the node planes do not interact with each other. Obviously, the absence of interaction is guaranteed if the perturbation ranges do not overlap, i.e., for node planes more than $2\times18=36$ monolayers away (wavelength $\lambda=72$ monolayers, $q/a^*=0.972$). In the inset of Fig. 5, however, we observe linear behavior over a much larger interval down to a separation of 24 monolayers between the node planes (wavelength $\lambda=48$ monolayers, $q/a^*=0.958$).

2. Confrontation with LDA+U data

We now examine whether or not in our LDA+U calculations we find similar properties for the node-node interaction as Uzdin and Demangeat found in their PAM study. APW+lo calculations for wavelengths longer than 40 monolayers are very expensive. We have therefore only two such calculations in Fig. 5 ($\lambda=56$ or $q/a^*=0.964$ and $\lambda=80$ or $q/a^*=0.975$), plus the pure AF case ($\lambda=\infty$ or $q/a^*=1.00$). Due to item (c) above, node-node interaction is unlikely for $q/a^*>0.972$. Therefore, it is justified to extrapolate the line that connects our two data points at $q/a^*=0.975$ and $q/a^*=1.00$ and to consider this as the energy difference without node-node interaction. This line turns out to go perfectly through the point at $q/a^*=0.964$ ($\lambda=56$) and almost through the one at $q/a^*=0.95$ ($\lambda=40$). For shorter wavelengths, there is a clear deviation from the linear behavior. This shows that, according to LDA+U, node-node interaction sets in somewhat above a node-node separation of 20 monolayers ($\lambda=40$), a value that is in perfect agreement with the one of the model Hamiltonian [see (d)]. In contrast to Uzdin and Demangeat,[22] we were able to stabilize solutions with wavelengths smaller than 40 monolayers without applying an external field. It is clear from Fig. 5 that none of these cases follow the linear behavior anymore (=node-node interaction). For a wavelength of 20 monolayers or less, the magnetic moments collapse and an essentially nonmagnetic solution is obtained (see top part of Fig. 5 where the magnetic moment is given as a function of the wave vector).

The interpretation of the line in Fig. 5 is that as long as node planes are not interacting with each other, insertion of an extra node plane requires 152 meV per Cr atom in the unit cell (this value is determined by the slope of the line, see

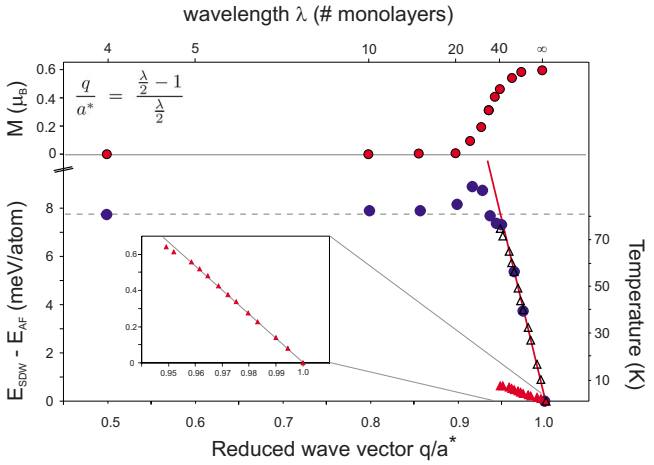

FIG. 5. (Color online) Bottom part: energy difference between the spin-density wave (E_{SDW}) and the antiferromagnetic configuration (E_{AF}) per atom as a function of wave vector (and wavelength). Our LDA+U data (circles) are compared with the PAM data of Uzdin and Demangeat (Ref. 22) (triangles), the latter in their original form [bottom of picture and inset modified (Ref. 37) from Ref. 22], as well as scaled to agree with our data. The data of Uzdin and Demangeat (Ref. 22) were fitted (solid line) with a function of the form $\Delta E/\mathrm{atom}=-E_{node}x+E_{node}$, where E_{node} is the formation energy per Cr atom for an isolated node plane (Sec. IV B). The dashed line indicates the energy difference between the nonmagnetic and the antiferromagnetic configurations. The temperature scale at the right-hand side is a tentative indication for the temperature it requires to form node planes at a wavelength on the linear curves. In the top part of the figure the magnetic moments resulting from our calculations are shown.

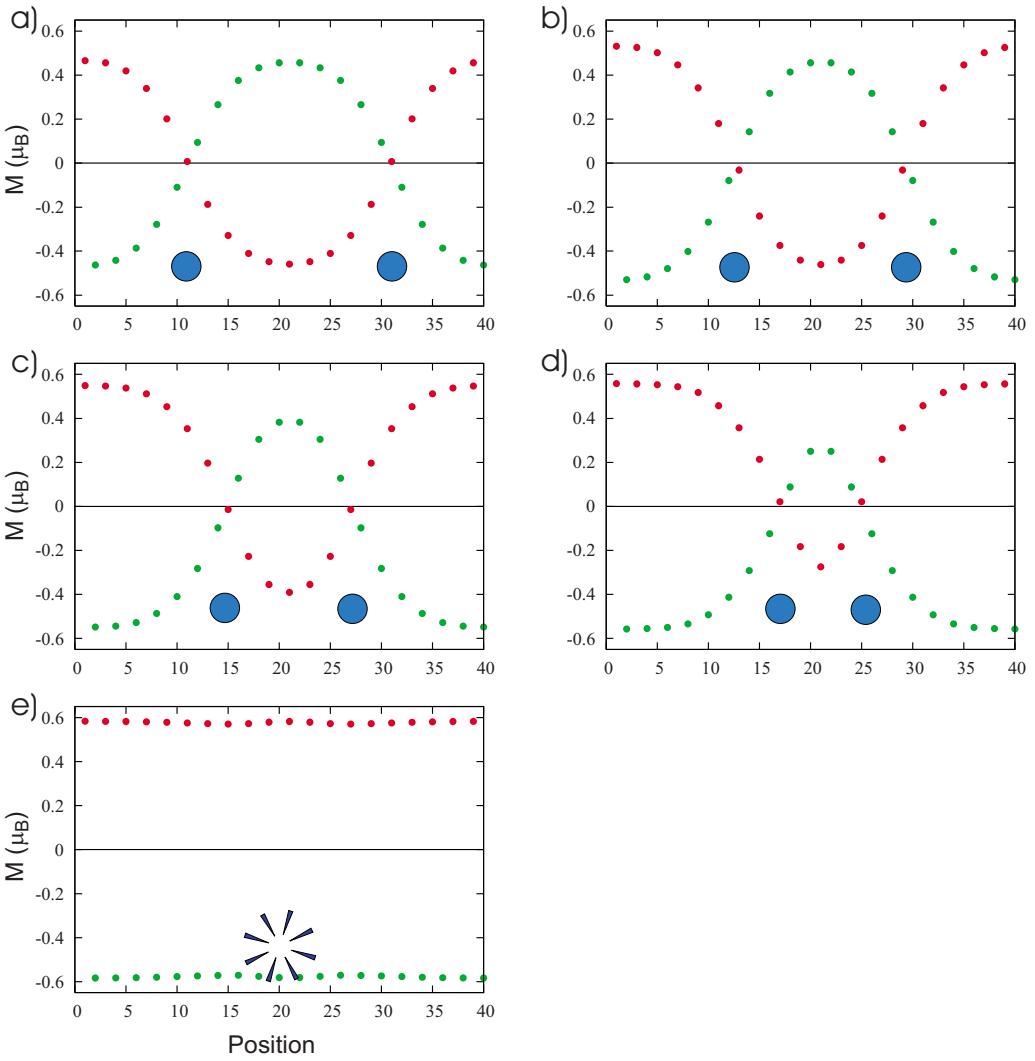

FIG. 6. (Color online) Magnetic moment profile as a function of node-node distance: (a) 20, (b) 16, (c) 12, (d) 8, and (e) 4 monolayers. The big circles give a visual impression of two approaching nodons which finally annihilate.

Sec. IV B for more details). With decreasing wavelength (=ever more node planes), the energy rises: for all wavelengths, the SDW state has an energy above the one of the AF state. As long as $\lambda \geq 32$ ($q/a^* \geq 0.9375$), the SDW state energy lies below the nonmagnetic state (dashed horizontal line in Fig. 5)—this is consistent with Fig. 1 for $\lambda = 40$. For wavelengths below 32 monolayers, the nonmagnetic state has a lower energy than the SDW state until the SDW state collapses below $\lambda = 20$ monolayers. In order to characterize better the kind of node-node interaction, we performed a series of calculations in a long AF cell, where two node planes are put at progressively smaller distances, leaving anything else antiferromagnetic. These calculations were (for efficiency reasons) performed in the $1 \times 1 \times 20$ supercell for node-node distances of 20, 16, 12, 8, and 4 monolayers and the corresponding wave profiles and the energy as a function of node-node distance are presented in Figs. 6 and 7, respectively. Figure 7 shows that an energy increase occurs when going from 20 to 16 monolayers, implying a *repulsive* node-node interaction for these distances. This confirms observation (a) in Sec. IV A 1. As soon as the node-node distance

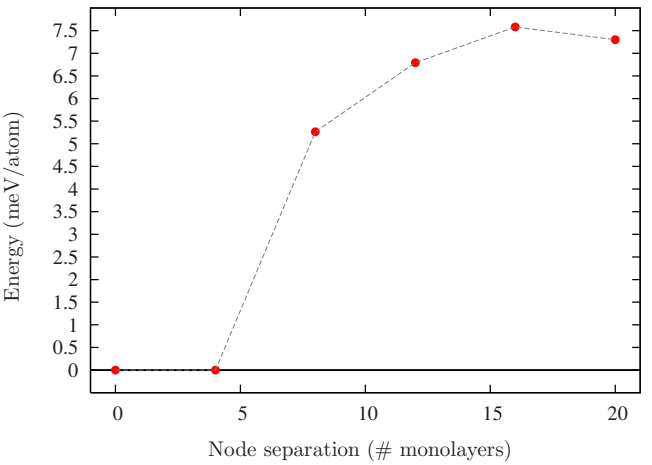

FIG. 7. (Color online) Energy per atom as a function of node separation. A separation of 0 monolayers evolved to the antiferromagnetic configuration. All energies are given with respect to the antiferromagnetic energy (=0 meV/atom).

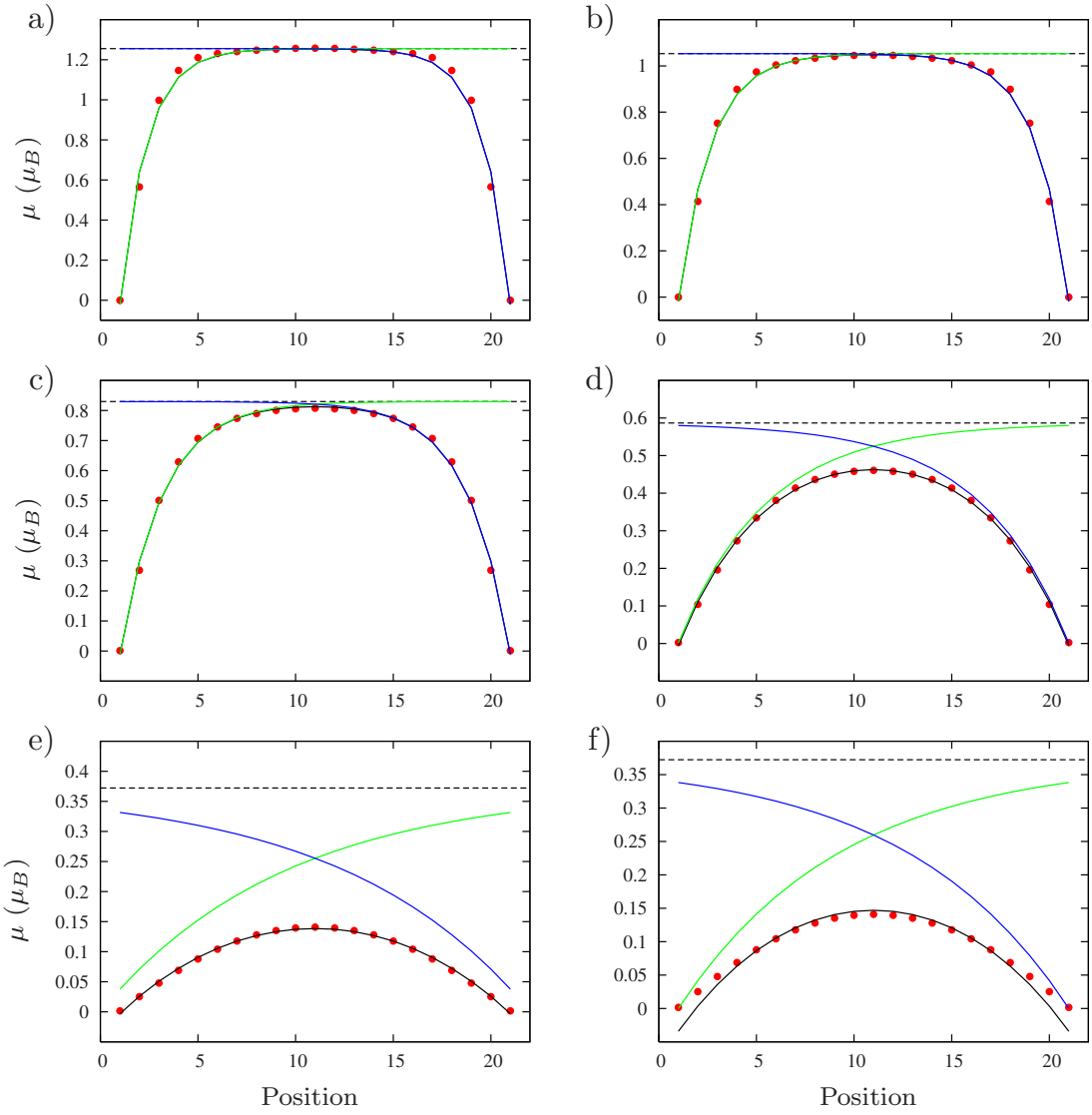

FIG. 8. (Color online) Fits of the spin-density wave with formula (2) for different lattice constants. (a) 2.96, (b) 2.91, (c) 2.86, (d) 2.80, and (e) 2.75 Å; (f) refit of the wave with a lattice constant of 2.75 Å with $\alpha=1$.

falls below 16 monolayers, the energy can be reduced by bringing the nodes even closer together. When a node-node distance of 4 monolayers is reached, the nodes spontaneously disappear, resulting in the pure antiferromagnetic state [Fig. 6(e)]. In the language of Uzdin and Demangeat,[22] annihilation has occurred [observation (b)]. As Fig. 6(e) demonstrates, annihilation occurs once the moments in between the two nodes are too weak to sustain the wave. We can thus conclude, based on Figs. 7 and 6, that the node-node interaction is repulsive for node-node distances down to 16 monolayers and that node-node distances smaller than this ultimately lead to mutual annihilation.

What remains to be examined is the perturbation range of an isolated node plane [item (c) in Sec. IV A 1]. This will shed a different light on the interaction distance as well. By varying the lattice constant, we have performed a series of LDA+U calculations as a function of the magnetic moment, all for an SDW wavelength of 40 monolayers. The energy versus lattice constant and the magnetic moment versus lattice constant curves for these calculations were already shown in Figs. 1 and 2, while the wave profiles for the different lattice constants (and thus magnetic moments) are given in Fig. 8. Fitting these data with a function that describes the disturbance of the magnetic moments in between the nodes will not only enable us to determine the perturbation range for a wave with the experimental amplitude, it also provides new information: the influence of the size of the moment on the perturbation range.

Visual inspection of Fig. 8 and of similar figures in Refs. 9 and 22 learns that an isolated node plane disturbs the surrounding Cr moments more or less in an exponential way,

$$M(x) = A_{\mathrm{AF}}(1 - \alpha e^{-(x-1)/d}), \tag{1}$$

where A_{AF} is the antiferromagnetic moment when no spin-density wave is present. The variable x counts the monolayers (the node plane appears at $x=1$) and the "relaxation distance" d is a measure for the searched perturbation range d_{per}. The parameter α will be discussed later and is currently set to 1. If the node planes are repeated every 20 monolayers,

the moments between two *distant* node planes are found as a simple superposition of the effect of two isolated node planes,

$$M(x) = A_{\mathrm{AF}}[1 - \alpha(e^{-(x-1)/d} + e^{(x-1-20)/d})] \quad (2)$$

with α still being unity. This is the case for the waves with high magnetic moments. Fits using Eq. (2) for these waves are shown in Figs. 8(a) and 8(b) and the fit parameters are given in Table I. The perturbation distance d_{per} can be extracted from the exponential decay parameter d in formula (2) as follows: one can estimate the perturbation distance for the wave at lattice constant 2.96 Å from Fig. 8(a) and thus obtain $d_{\mathrm{per}}=5.0d$ (last column in Table I). If the perturbation range becomes larger than half of the distance between two node planes, the node planes can in principle interact [Figs. 8(c) and 8(d)]. The fact that, in such cases, we can still use Eq. (2) with $\alpha=1$—i.e., the moment profile is just a superposition of the moment profiles due to isolated node planes—is an indication that nevertheless these node planes do not interact. This is consistent with our earlier conclusions. Finally, if the perturbation range extends over the neighboring node plane [Figs. 8(e) and 8(f)], then a superposition as in Eq. (2) with $\alpha=1$ cannot work anymore (the moment at the nodes should become negative). Still, a fit with Eq. (2) with α as a free parameter gives a reasonable description of the data [Fig. 8(e)]. Combining all these observations leads to the conclusion that the perturbation range increases with decreasing magnetic moment. Moreover, for magnetic moments close to (in our case, a bit smaller than) the experimental value interaction occurs when the node-node distance becomes smaller than the experimentally observed period for low temperatures. This is in agreement with the two data sets shown in Fig. 5.

Additionally, the wave profiles in Fig. 8 offer a different view on the origin of higher harmonics in the SDW state. It is experimentally[2,38,39] known that the wave modulation is not described by a single cosine, but that a small third-order harmonic is present as well. Even harmonics are excluded by symmetry. The experimental ratio between the amplitude of the first (M_1) and third (M_3) harmonic is −0.016 (Ref. 38) or −0.021.[2] The wave form is triangular for positive M_3/M_1, which means that the antinodes of the fundamental wave and the third harmonic have the same sign where they coincide, and rectangular for negative M_3/M_1, where they have opposite sign at the antinodes. From Fig. 8(c), it is seen that such an almost cosinelike shape naturally arises from the superposition of two exponential moment profiles. Also the increase of $|M_3/M_1|$ with increasing magnetic moment of the SDW (=the wave becomes more squarelike) as observed in previous calculations[8,9,21] gets a natural explanation: a short perturbation range and a region halfway two nodes where the original AF moments are not affected are equivalent to a squarelike wave.

B. Formation energy of node planes

A crucial feature in the nodon model is the asymmetric potential of Fig. 4 for the creation, destruction, and displacement of a single node. Can we quantify some features of this potential? Calculating the energy difference between the antiferromagnetic state and a case with a single isolated node would require a calculation for a supercell large enough to prevent interaction with nodes in neighboring supercells in all directions. As the interaction range of a node *plane* was found to be quite large (see Table I), it can be expected that the influence of a single node is felt over a significant distance as well. We did not attempt to calculate such large supercells. Instead, we look at the effective energy needed to form an isolated node plane starting from the AF state and ignoring the unknown transition energy barrier in Fig. 4. This information can be read from Fig. 5. Starting from the AF state at the right-hand side of this picture, all other data points represent the increase in energy by adding progressively more node planes to the original AF state. Before interpreting Fig. 5, we first explain in detail how it is built: Consider a unit cell for a SDW with wavelength λ. The length of this unit cell must be an integer multiple n of the wavelength (n is not necessarily 1), and the cell contains $2n$ node planes and $n\lambda$ atoms (λ is given in number of monolayers as before). If the energy difference between this cell and an AF cell with the same number of atoms is called ϵ, then $\epsilon/(2n)$ is the energy increase per node plane when AF Cr is converted into SDW Cr with wavelength λ (or more precisely the energy increase per Cr atom that is part of a node plane because due to periodic boundary conditions in the plane perpendicular to the wave vector only one Cr atom in the unit cell is needed to represent the node plane). Once the wavelength is large enough to prevent interaction between the node planes, $\epsilon/(2n)$ becomes a constant. This constant can be interpreted as the energy (per Cr atom of the node plane) that is needed to introduce a single isolated node plane into AF Cr. Graphically, it is the opposite of the *slope* of the linear part in Fig. 5. Conversely, as long as the data in Fig. 5 remain linear ($0.95 < q/a^* \leq 1$ for our LDA+U calculations) we can conclude that there is no interaction between node planes for that wavelength. What is given as the vertical axis of Fig. 5 is $\epsilon/(n\lambda)$: the overall energy difference per atom of the considered unit cell.

Predictions for the energy required to create a single node plane turn out to depend strongly on the computational method that is used. The PAM results by Uzdin and Demangeat are shown at the very bottom and in the inset of Fig. 5. They form a straight line in the interval $0.958 \leq q/a^* \leq 1$, which indicates that there is no interaction between node planes for wavelengths beyond 48 monolayers

TABLE I. Fit parameters obtained by least-squares fits of the calculated data with function 2.

Lattice constant (Å)	A_{AF} (μ_B)	α (μ_B)	d	$d_{interaction}$ (No. of monolayers)
2.75	*0.373*	*1*	*8.4(1)*	*42(9)*
2.75	0.373	0.899(4)	9.5(1)	48(7)
2.80	0.584	0.998(5)	4.45(3)	22(3)
2.86	0.830	1.01(1)	2.18(4)	11(2)
2.91	1.052	1.02(1)	1.66(4)	8(1)
2.96	1.255	1.02(2)	1.37(5)	7(1)

(see also Sec. IV A 1). The opposite of the slope of this line is 13.5 meV/nodon, which is the PAM prediction for the energy to create an isolated node plane. In order to get a feeling for the magnitude of this number, it is instructive to convert it to temperature as follows: divide it by the number of Cr atoms that are closer to this node plane than to any other node plane in order to get an energy per atom (=divide by 20 if $\lambda=40$, which would give here $13.5/20=0.67$ meV/atom). By the conversion 1 meV/atom $\rightarrow 10$ K, this gives about 7 K to obtain the SDW with the experimental wavelength ($\lambda=40$)—see the right axis of Fig. 5. For smaller densities of node planes (=larger λ), this temperature becomes smaller. The same value predicted by LDA+U is two orders of magnitude larger, as is graphically obvious from Fig. 5: 152 meV/nodon (≈ 76 K to obtain the experimental SDW). From earlier LDA and GGA calculations, a value of 47 meV/nodon (≈ 23 K) can be determined if the moment is forced to be identical to the experimental moment (Fig. 3 in Ref. 21). If the large GGA moment is allowed, the nodon formation energy is 160 meV/atom (≈ 80 K) (Fig. 3 in Ref. 21). The latter two values show that introducing a zero moment region (=a node plane) in a sea of AF moments becomes more difficult if the moments that have to be killed are larger. As in our LDA+U calculations the moment (measured as the wave amplitude at $\lambda=40$, as in Fig. 3 in Ref. 21) is somewhat smaller than the experimental value, one would have expected a correspondingly smaller nodon formation energy here. The observation that it is rather large means that the LDA+U moments are harder to kill than LDA or GGA moments, an observation which we take here without further attempt to explain. In any case, these three numbers give the range of nodon formation energies predicted by *ab initio* methods as roughly 50–150 meV/nodon ($\approx 20-80$ K). This formation energy corresponds to the double-sided arrow in Fig. 4. As the interaction between different nodes within one node plane is attractive, this value is a *lower bound* for the energy needed to create an individual node.

Although the characteristic temperature for the spontaneous formation of nodons as predicted by PAM (≈ 7 K) is one order of magnitude smaller than the temperature predicted by *ab initio* methods ($\approx 20-80$ K), even the latter values are still well below the Néel temperature of Cr (311 K) (see also conclusion vii in Ref. 9). This implies that this *ab initio* information is consistent with the interpretation of the SDW in Cr as due to thermal excitation of nodons. It is not necessarily true that nodon formation should happen in the bulk of Cr, as was implicitly understood so far. One could imagine that nodon formation happens predominantly at intrinsic defects, which could offer them a reduced formation energy—similarly to CO_2 bubbles in a glass with sparkling water, which originate at imperfections of the wall. In such a scenario, the characteristic formation temperature could be considerable lower than the 20–80 K estimated here for bulk Cr, which would be even more easy to reconcile with the experimental observations.

V. CONCLUSIONS

The works by Hafner *et al.*[9] and by Uzdin and Demangeat[22] have shifted the point of view on the SDW in Cr from a wave of magnetic moments to holes in an antiferromagnetic background. Those holes can be understood as low-lying excitations (nodons) of the antiferromagnetic ground state. In the present paper, we want to stir the discussion on this potentially useful alternative viewpoint by examining whether *ab initio* methods predict the required properties for these nodons. We extract this information not only from LDA and GGA calculations (which both have known deficiencies for describing SDW Cr) but also from LDA+U calculations that offer a more consistent description of Cr. Our calculations indicate that nodons do not interact with each other if they are separated by somewhat more than 20 monolayers. They repel each other when they are between 16 and 20 monolayers apart. Bringing nodons closer than 16 monolayers from each other ultimately leads to annihilation. The presence of a node plane perturbs the moments of the neighboring Cr atoms up to 18 monolayers away from the plane. A characteristic temperature at which nodons are formed by thermal fluctuations can be estimated to be 20–80 K. This is considerably larger than what is predicted by a model Hamiltonian (7 K) but still low enough to leave the possibility open for the nodon model to be a valid description of the SDW in Cr. A suggestion for further work that could increase the insight in this problem is to make simulations with a three-dimensional lattice gas model using particles that have the properties of the nodons. Do they indeed organize themselves in node planes? What is the equilibrium distance between planes? Does this distance increase with increasing temperature? We hope that our present analysis will encourage further research on the nature of the SDW in Cr, the question of the actual ground state of Cr, and the ability of condensed matter theory to model and/or predict this ground state.

ACKNOWLEDGMENTS

The authors have benefited from helpful discussions with M. Richter, R. Callens, C. L'abbé, and J. Meersschaut. This work was supported by the Fund for Scientific Research—Flanders (FWO) (Projects No. G.0239.03, No. G.0447.05, and No. G.0191.08), the concerted action of the K.U. Leuven (Grant GOA/2004/02), the Centers of Excellence Programme of the K.U. Leuven (INPAC, Grant No. EF/05/005), and the Belgian Interuniversity Attraction Pole program (Grant No. IAP P6/42). This research made use of VIC, the HPC infrastructure of the K.U. Leuven.

*stefaan.cottenier@ugent.be

[1] S. A. Werner, A. Arrott, and H. Kendrick, Phys. Rev. **155**, 528 (1967).
[2] E. Fawcett, Rev. Mod. Phys. **60**, 209 (1988).
[3] J. Kübler, *Theory of Itinerant Electron Magnetism*, 1st ed. (Clarendon Press, Oxford, 2000).
[4] R. M. White, *Quantum Theory of Magnetism*, 2nd ed. (Springer-Verlag, Heidelberg, 1983).
[5] A. W. Overhauser, Phys. Rev. **128**, 1437 (1962).
[6] W. M. Lomer, Proc. Phys. Soc. London **80**, 489 (1962).
[7] J. Schäfer, E. Rotenberg, S. D. Kevan, and P. Blaha, Surf. Sci. **454-456**, 885 (2000).
[8] R. Hafner, D. Spišák, R. Lorenz, and J. Hafner, J. Phys.: Condens. Matter **13**, L239 (2001).
[9] R. Hafner, D. Spišák, R. Lorenz, and J. Hafner, Phys. Rev. B **65**, 184432 (2002).
[10] M. Bayer, Master thesis, Leibniz-Institut für Festkörper- und Werkstofforschung Dresden, 2008. Available at http://www.ifw-dresden.de/institutes/itf/diploma-and-phd-theses-at-the-itf/mathias_bayer_diplom.pdf
[11] J. Kübler, J. Magn. Magn. Mater. **20**, 277 (1980).
[12] J. Chen, D. Singh, and H. Krakauer, Phys. Rev. B **38**, 12834 (1988).
[13] V. L. Moruzzi and P. M. Marcus, Phys. Rev. B **42**, 8361 (1990).
[14] V. L. Moruzzi and P. M. Marcus, Phys. Rev. B **46**, 3171 (1992).
[15] D. J. Singh and J. Ashkenazi, Phys. Rev. B **46**, 11570 (1992).
[16] P. M. Marcus, S.-L. Qiu, and V. L. Moruzzi, J. Phys.: Condens. Matter **10**, 6541 (1998).
[17] K. Hirai, J. Phys. Soc. Jpn. **66**, 560 (1997).
[18] K. Hirai, J. Phys. Soc. Jpn. **67**, 1776 (1998).
[19] G. Y. Guo and H. H. Wang, Phys. Rev. B **62**, 5136 (2000).
[20] G. Bihlmayer, T. Asada, and S. Blügel, Phys. Rev. B **62**, R11937 (2000).
[21] S. Cottenier, B. D. Vries, J. Meersschaut, and M. Rots, J. Phys.: Condens. Matter **14**, 3275 (2002).
[22] V. M. Uzdin and C. Demangeat, J. Phys.: Condens. Matter **18**, 2717 (2006).
[23] E. Sjöstedt, L. Nordström, and D. Singh, Solid State Commun. **114**, 15 (2000).
[24] G. K. H. Madsen, P. Blaha, K. Schwarz, E. Sjöstedt, and L. Nordström, Phys. Rev. B **64**, 195134 (2001).
[25] S. Cottenier, *Density Functional Theory and the Family of (L)APW-Methods: A Step-by-Step Introduction* (K.U. Leuven, Leuven, 2002) (to be found at http://www.wien2k.at/reg_user/textbooks).
[26] P. Hohenberg and W. Kohn, Phys. Rev. **136**, B864 (1964).
[27] W. Kohn and L. Sham, Phys. Rev. **140**, A1133 (1965).
[28] P. Blaha, K. Schwarz, G. Madsen, D. Kvasnicka, and J. Luitz, WIEN2k, *An Augmented Plane Wave+Local Orbitals Program for Calculating Crystal Properties* (Technische Universität Wien, Vienna, 1999).
[29] U. von Barth and L. Hedin, J. Phys. C **5**, 1629 (1972).
[30] D. M. Ceperley and B. J. Alder, Phys. Rev. Lett. **45**, 566 (1980).
[31] S. H. Vosko, L. Wilk, and M. Nusair, Can. J. Phys. **58**, 1200 (1980).
[32] J. P. Perdew, K. Burke, and M. Ernzerhof, Phys. Rev. Lett. **77**, 3865 (1996).
[33] M. T. Czyżyk and G. A. Sawatzky, Phys. Rev. B **49**, 14211 (1994).
[34] E. P. y Blancá, J. Desimoni, N. E. Christensen, H. Emmerich, and S. Cottenier, Phys. Status Solidi B **246**, 909 (2009).
[35] S. J. Hashemifar, N. Ghaderi, S. Sirousi, and H. Akbarzadeh, Phys. Rev. B **73**, 165111 (2006).
[36] G. W. Fernando, R. E. Watson, M. Weinert, A. N. Kocharian, A. Ratnaweera, and K. Tennakone, Phys. Rev. B **61**, 375 (2000).
[37] The original PAM data were given per *d* electron, V. Uzdin (private communication), and need to multiplied by 5 to be compared with the *ab initio* data. The factor Γ that is needed for the conversion is estimated to be 0.6 eV.
[38] R. Pynn, W. Press, S. M. Shapiro, and S. A. Werner, Phys. Rev. B **13**, 295 (1976).
[39] S. Iida, Y. Tsunoda, and Y. Nakai, J. Phys. Soc. Jpn. **50**, 2587 (1981).